Turkish Journal of Electrical Engineering & Computer Sciences

http://journals.tubitak.gov.tr/elektrik/

Research Article

Turk J Elec Eng & Comp Sci
(2017) 25: 3660 – 3672

doi:10.3906/elk-1604-222

# Effect of uniform and Dolph–Chebyshev excitations on the performance of circular array antennas

**Mohan KACHALAI NARSIMMAN[1,*], Yogesh Kumar CHOUKIKER[1], Srinivasa Rao ZINKA[2], Kannadassan DHANARAJ[1]**

[1]School of Electronics Engineering, VIT University, Vellore, India

[2]Department of Electrical & Electronics Engineering, BITS Pilani, Hyderabad, India

**Received:** 18.04.2016 • **Accepted/Published Online:** 27.05.2017 • **Final Version:** 05.10.2017

**Abstract:** This paper presents the design and simulation of microstrip circular antenna arrays and studies the effect of excitation with uniform and Dolph–Chebyshev distribution. With side lobe level of 20 dB and 8 microstrip circular patches, the circular array has been demonstrated with minimum grating lobes. The effects of patch and antenna array length on directivity, radiation patterns, and side lobe are also studied in detail. It is found that these antenna arrays are suitable for radar application.

**Key words:** Circular patch, circular ring, radar, side lobe level

## 1. Introduction

Circular antenna arrays (CAAs) have many potential applications in wireless technology such as radar and satellite [1,2]. While comparing other planar arrays, like rectangular arrays, CAAs are beneficial as they have flexible and symmetric radiation patterns [3], have full azimuth scan capability [4,5], are nearly omnidirectional [6], and are conformal to the surface. CAAs can be designed with a fixed main beam or a scanning beam, which is rapidly positioned in direction with the help of electromechanical devices. These devices change the phase between radiators to produce the expected phase progression along the array.

CAAs are classified as circular ring antenna arrays in general planar arrays [7,8]. There are other configurations that were proposed in circular arrays, namely circular planar array and concentric circular antenna array. In this paper, we have considered only the circular (ring) antenna arrays. CAAs have been studied in various aspects, such as analytical mathematical modeling of array factor (AF), nonuniform excitation of elements [9], optimization of configuration for beam-forming, high directive applications [10], and optimization of radiation pattern to achieve improved side-lobe levels [11,12]. Works are also carried out towards interelement mutual coupling with limited numbers of antenna elements [13,14] and frequency independent arrays [15]. Recently, Zinka et al. have demonstrated various numerical simulations of planar and circular arrays to figure out outcomes of various configuration and excitation [16,17]. They also proposed a unique simulation tool called ARRAYTOOL.

ARRAYTOOL is a Python-based tool box for antenna array systems. It calculates the radiation pattern in 2D and 3D space using discrete/continues Fourier transform, to study and analyze the array of radiation. The tool is aimed to have varying flexibility, such as linear-planar-circular arrays with variable nonuniform

*Correspondence: narasimmamohan@gmail.com

excitation coefficients, nonuniform excitation phase, nonuniform element spacing, and phase modes for circular arrays. The tool is open source and available in [16]. In the near future, the beam-forming, directional of arrival, and target detection algorithms will be included. A detailed discussion on various programing aspects of ARRAYTOOL is presented in [16,17].

Nonuniform excitation of antenna array elements is a common technique to suppress the side-lobe level and improve the directivity. Analytical methods for sum patterns such as Chebyshev or Taylor polynomials are widely used for uniformly spaced linear arrays with isotropic elements. Dolph originally introduced Chebyshev polynomials for the excitation of isotropic antenna arrays to achieve equal leveled side lobes [18]. The design procedure of Dolph–Chebyshev (DC) arrays is outlined in reports including [19] and [20]. The DC patterns have many advantages like controlled side lobe level (SLL) or trade-off between SLL and number of elements. However, either SLL or beam width can be used as a design parameter, not both. The synthesis and computational techniques of current distribution for DC patterns of linear arrays are developed by various authors [21,22]. Thadeu et al. have demonstrated a modified Chebyshev pattern synthesis method to overcome such a limitation [23]. Recently, DC arrays are useful for various applications. Liu et al. have demonstrated in $1 \times 8$ conical array with DC distribution with a high gain of 15.9 dB [24]. In this work, the power division to each element was managed with a Wilkinson power divider to achieve a high SLL of 30 dB. For high performance defense applications, planar conformal microstrip array of $18 \times 14$ elements with DC excitation was reported by Zhang et al. The DC distribution of power for 84 elements was designed using a Wilkinson power divider, which results in a HPBW of $8^\circ$ and a decent SLL of 17 dB [25].

CAAs with nonuniform excitation are rarely reported. The concept of nonuniform excitation in circular arrays was introduced by Davies. He demonstrated the computation of current distributions for CCAs from linear arrays (LAs) using phase transformation [26]. Later this technique was further developed for smooth direction finding applications by Rahim et al. [3], which is basically to transform the array element space to mode space, also called 'spatial harmonics' or 'virtual array'. Lau et al. have reduced the complexity of implementation of DC pattern synthesis, which allows nonisotropic elements [27]. This work was inspired by Tseng et al.'s method to design arbitrary arrays [20]. They also have reported various advantages of the method, including the incorporation of mutual coupling effects between elements, iterative adaptive array approach with recalculation of weights based on look-up angles, and incorporation of nonisotropic elements with nonuniform excitation without complex calculations [27].

Circular microstrip patch-based CAAs with uniform excitation have been reported [28,29]. Among the various patch structures, the circular patch has improved radiation symmetry and improved bandwidth. In this paper, we present the design, synthesis, and simulation of a DC uniform circular array with circular patch elements using phase mode theory; the uniform and DC excitation coefficients are calculated numerically. The simulation of the circular patch array is also demonstrated with a gain in the design frequency of 10 GHz.

## 2. Design of single circular patch antenna element

The circular patch design was proposed by various authors as linearly and circularly polarized radiators [30–32]. A successful analytical model was reported using the radiating structure by Shen et al. and expressed the analytical formula for the resonant frequency [33]. Richmond's reaction technique and uni-moment - Monte Carlo method have described the resonance frequency of the patch in [34]. Derneryd et al. proposed the most accurate formula for the resonant frequency with approximation of the capacitance as a function of patch

dimensions [35]. The simple and effective design methodology of a circular patch for each mode is presented in [12]. The radius of the patch is

$$R = \frac{F}{\left\{1 + \frac{2h}{\pi\varepsilon_r F}\left[\ln\left(\frac{\pi F}{2h}\right) + 1.7726\right]\right\}^{\frac{1}{2}}}, \tag{1}$$

where

$$F = \frac{8.791 \times 10^9}{f_o\sqrt{\varepsilon_r}}$$

For the design frequency of 10 GHz, the patch radius is calculated as $R$ =0.525 cm for the RT duroid 5880 ($\varepsilon_r$= 2.2) substrate and height $h$ = 0.1588 cm. The circular patch element is created on top of the substrate and fed by a coaxial cable as shown in the inset of Figure 1. Electric and magnetic conductors are placed at the top and bottom of the substrate. The magnetic conductor is placed around the circular peripheral of the cavity. The proposed design has the advantage of simplicity and the positioning of the feed point. HFSS EM tool is used to simulate the patch antenna. Figure 1 shows the return loss characteristics from EM simulation where the resonance occurred at frequency of 9.97 GHz. Figure 2 shows the E and H plane gain pattern of the circular patch. It ensures that the patterns are directional in nature and gain of the circular patch antenna is 7.51 dB at the resonance $f_o$. This circular patch with coaxial feed is used in CAAs as an array element.

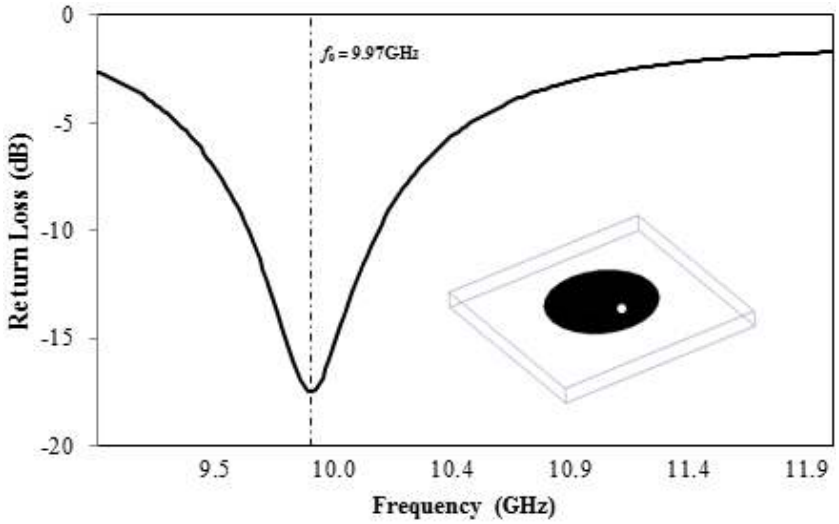


**Figure 1.** Return loss characteristics of single circular patch element (10 GHz); inset: schematic of circular patch with probe feed.

### 3. Uniform circular ring array

Consider $N$number of elements placed in a circular ring with rotational symmetry. The spacing between the elements is $d = \frac{\lambda}{4}$ ; therefore the circumference of the ring will be $Nd = 2\pi a$, where '$a$' is the radius of the circular ring. Figure 3 shows the element set-up in the circular array with center of array at origin. Now the far field pattern can be calculated by addressing the array factor (AF) and individual element's pattern. The AF of the circular ring array can be expressed as

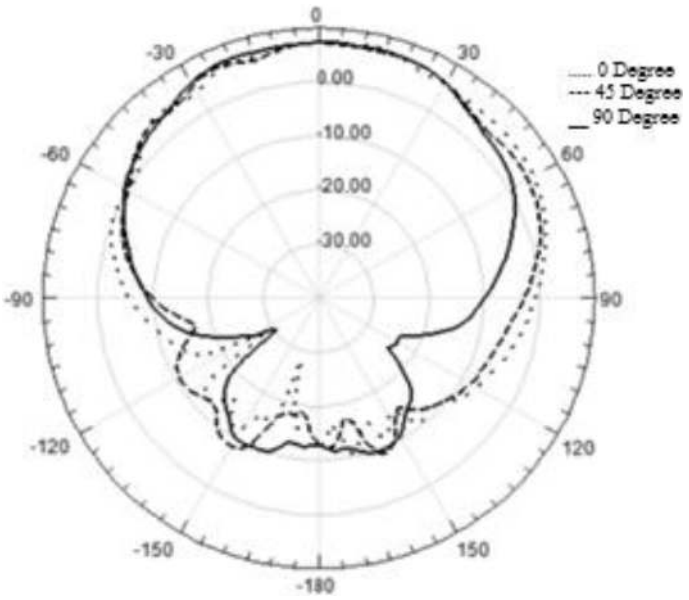


**Figure 2.** 2D gain pattern for single patch at $f_o = 9.97$ GHz for $\phi = 0^\circ; 45^\circ; 90^\circ$.

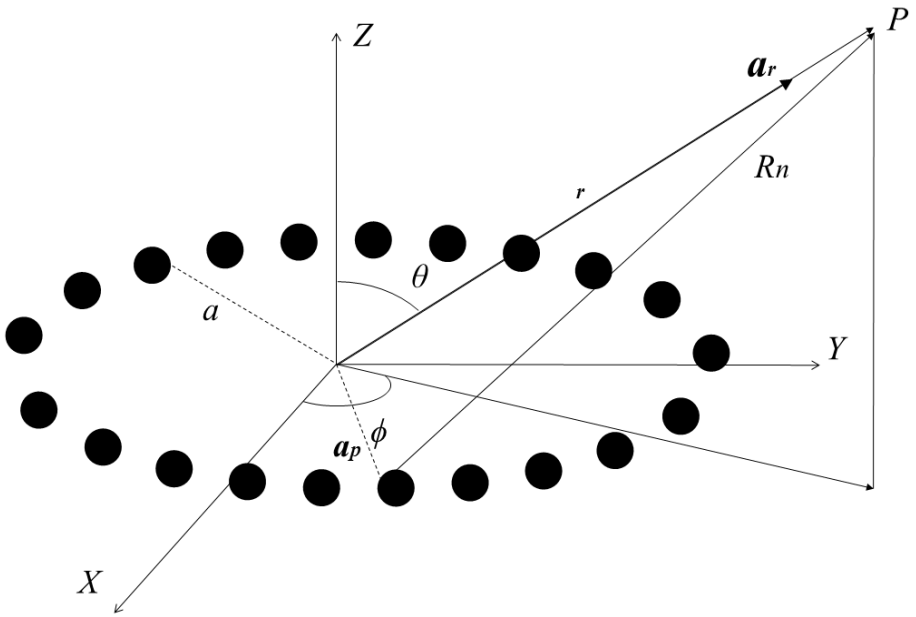


**Figure 3.** Far field coordinates for circular ring array.

$$E_n(r,\theta,\phi) = \sum_{n=1}^{N} J_n e^{\frac{-jkR_n}{R_n}}, \tag{2}$$

where $R_n$ is the far field distance from the nth element to point $P$; in general $R_n = \left(r^2 + a^2 - 2arcos\phi_n\right)^{\frac{1}{2}}$. While defining the coordinates of the circular ring, indeed it is difficult to represent the AF with a reference element. One can consider unit radical vector $\hat{a_r}$, $\hat{a_p}$ is the unit vector of line $\vec{OP}$. $R_n$ is the distance of point $P$ from the nth element of the circular array. The total field due to all elements can be calculated by angles of

line $R_n$ for each element $\phi_n$ with respect to the $x$-axis,

$$E_n(r,\theta,\phi) = \frac{e^{-jkr}}{r}\sum_{n=1}^{N} J_n e^{+jkasin\theta cos?(\phi-\phi_n)} \tag{3}$$

Due to the circular nature of the array, the weight function and the far-field antenna pattern are periodic functions with period $2\pi$. The $J_n$ is finite Fourier pair of an excitation coefficient (phase and amplitude) of the nth element

$$J_n = \frac{1}{2\pi}\int_0^{2\pi} E_n(r,\theta,\phi)e^{-jkasin\theta cos(\phi-\phi_n)}d\phi_n$$

This can be written as

$$J_n = V_n e^{j\alpha_n}, \tag{4}$$

where $V_n$ and $\alpha_n$ are magnitude and phase of excitation at the nth element, respectively. Substituting Eq. (4) in Eq. (3) results in

$$E_n(r,\theta,\phi) = \frac{e^{-jkr}}{r}\sum_{n=1}^{N} V_n e^{+jkasin\theta\cos(\phi-\phi_n)+\alpha_n} \tag{5}$$

This equation is normalized to write the AF. Along with the excitation coefficient, the calculation of AF is quite challenging with various phase differences. Finally, the AF for circular array of $N$ number of elements can be written as

$$AF(\theta,\phi) = \sum_{n=1}^{N} V_n e^{ika(cos\varphi-\varphi_{o)}}, \tag{6}$$

where

$$AF(\theta,\phi) = \sum_{n=1}^{N} V_n e^{ijka[sin\theta\cos(\phi-\phi_n)-sin\theta\cos(\phi-\phi_o)]}$$

These equations are programmed and simulated using ARRAYTOOL [16]. In the broadside case, the $\theta_o$ and $\phi_o$ are specified as $90^\circ$ and $0^\circ$, respectively. In general, the AF is associated with a zero order Bessel function called the principle term. The higher order terms are negligible. Readers are recommended to visit the website as in [16] to know more about ARRAYTOOL. Figures 4 and 5 show the isotropic excitation of CA and the corresponding radiation pattern for $N = 8$. These results are obtained from ARRAYTOOL.

## 4. Uniform and DC microstrip circular array

### 4.1. Uniform excitation

A microstrip circular array antenna (MCAA) is designed with microstrip circular patches in a ring of radius $a$ on substrate as shown in Figure 6. In the circular array, the element spacing between the patches is considered as $d = 1.35\lambda$ and $d = 0.67\lambda$ for 4 and 8 element MCAAs, respectively, for the radius of the ring $a = 2.6$ cm. In the case of a 16 element array, the spacing $d = 0.33\lambda$ and ring radius $a = 5$ cm are taken to avoid overlapping of the elements. These MCAAs are simulated for the same simulation environment in HFSS as that of a single element.

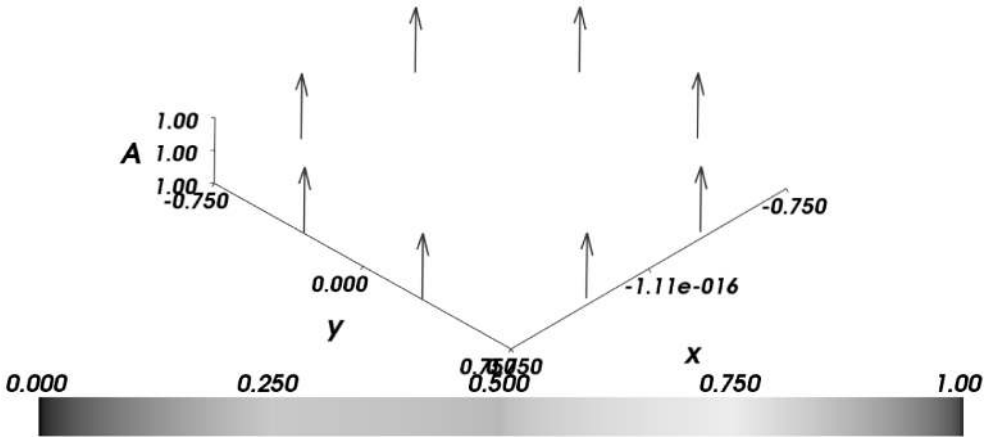


**Figure 4.** Uniform excitation of isotropic circular array for $N = 8$.

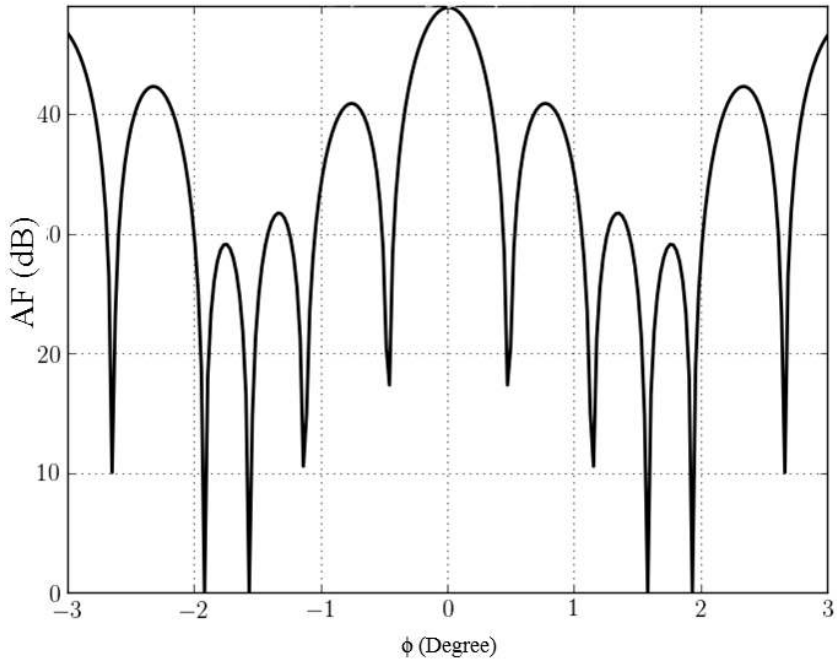


**Figure 5.** Radiation pattern of $N = 8$ isotropic circular array.

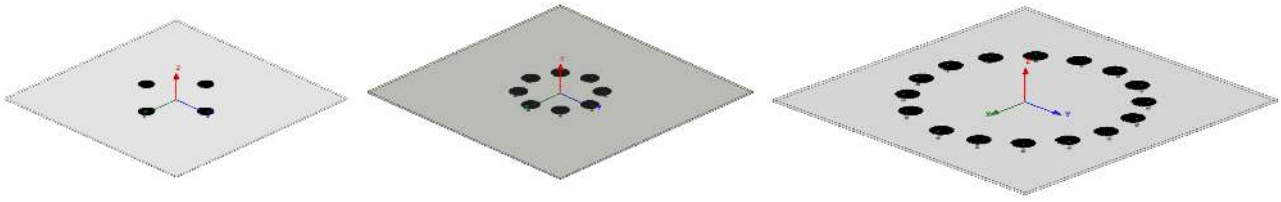

**Figure 6.** Configuration of 4, 8, and 16 microstrip in EM tool.

Figure 7 shows the two-dimensional radiation pattern of all MCAA $\phi = 90^\circ$ plane. At the resonance, the directive gain is 10.41 dB with HPBW of 28°. A visible difference can be found between each principle cuts plane. While $\phi = 0^\circ$ and 45° patterns are identical, the pattern at $\phi = 45^\circ$ shows a clear difference in

nulls. This large difference between side lobe levels and null position indicates that the grating lobes are formed between first side lobes as shown in Figure 8. This is due to large spacing between the interelements. These speculations are addressed with radiation characteristics of 8 and 16 element MCAAs.

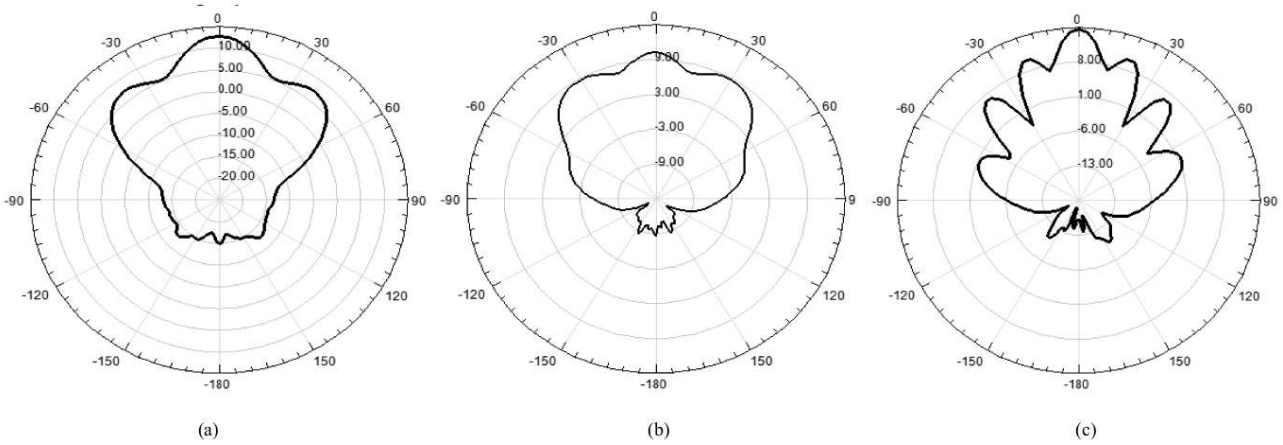


**Figure 7.** 2D gain pattern of MCAA for $f_o = 9.97$ GHz for $\phi = 90^\circ$, (a) 4 elements, (b) 8 elements, (c) 16 elements.

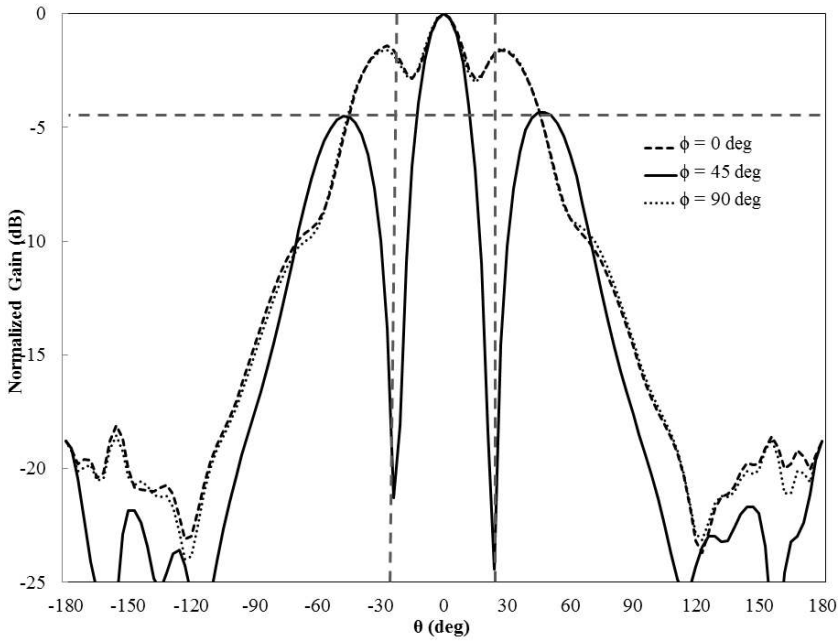


**Figure 8.** Gain pattern of 4 element MCAA at $f_o = 9.97$ GHz for various azimuthal angles.

Figures 9 and 10 show the normalized gain patterns of 8 and 16 MCAAs, respectively, at different principle cut planes. All patterns are identical, which reveals that there is no formation of grating lobes. These results clearly show that the large spacing between the elements is responsible for grating lobes. These patterns have the SLL of 25 dB at $90^\circ$, which is higher than that of the 4 element MCAAs. For the 16 element MCAA, the ring radius $(a)$ is twice that of the 4 or 8 element MCAAs. It is observed that the 16 element MCAA has three side lobes with exponentially decreasing SLLs within $\pm 60^\circ$. This is due to the lower element spacing and mutual coupling behind the elements. Figure 11 shows the mutual coupling between the elements for all arrays.

This coupling effect will be present when the spacing '$d$' between the elements is very small; it will affect the array radiation and matching characteristics of an antenna element. The mutual coupling is less because of the individual feed network. Table 1 summarizes the performance of MCAAs in terms of maximum gain, SLL, HPBW, and FNBW.

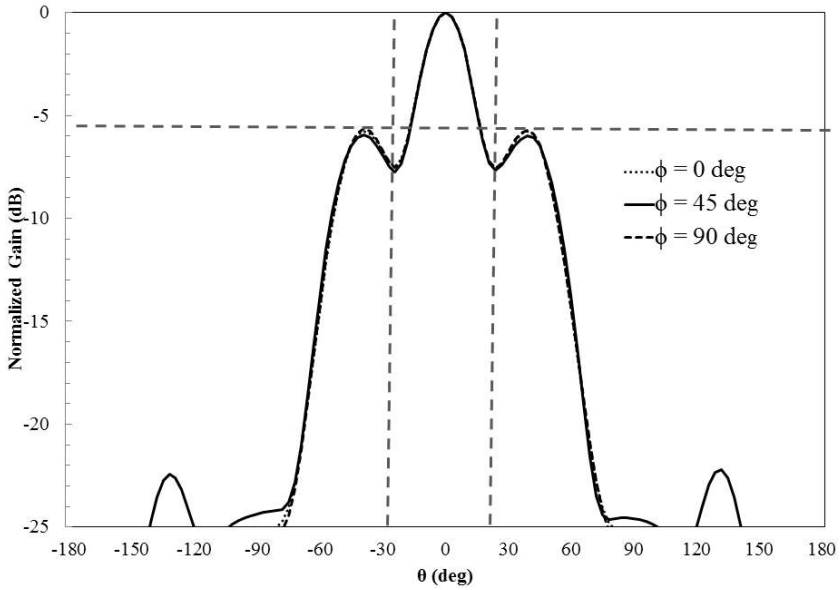


**Figure 9.** Gain pattern of 8 element MCAA at $f_o$ = 9.97 GHz for various azimuthal angles.

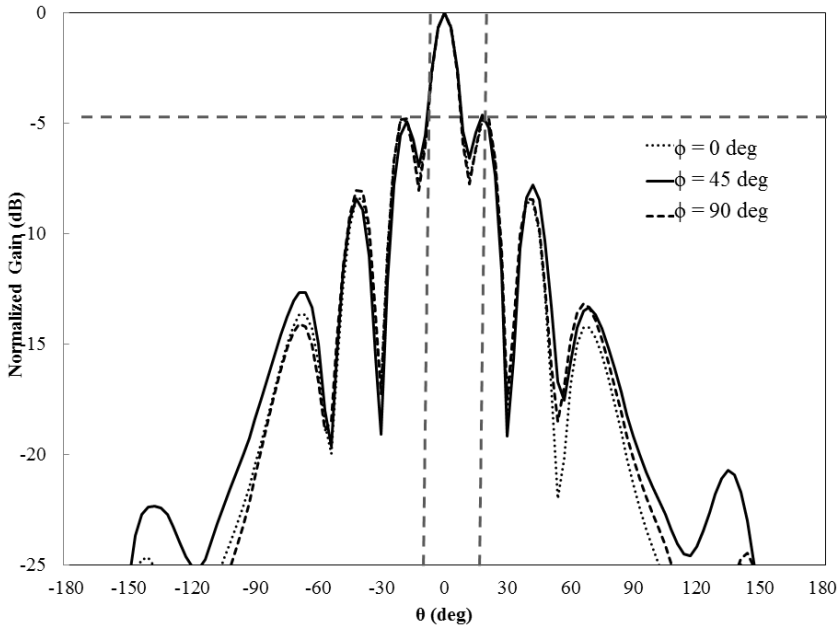


**Figure 10.** Gain pattern of 16 element MCAA at $f_o$ = 9.97 GHz for various azimuthal angles.

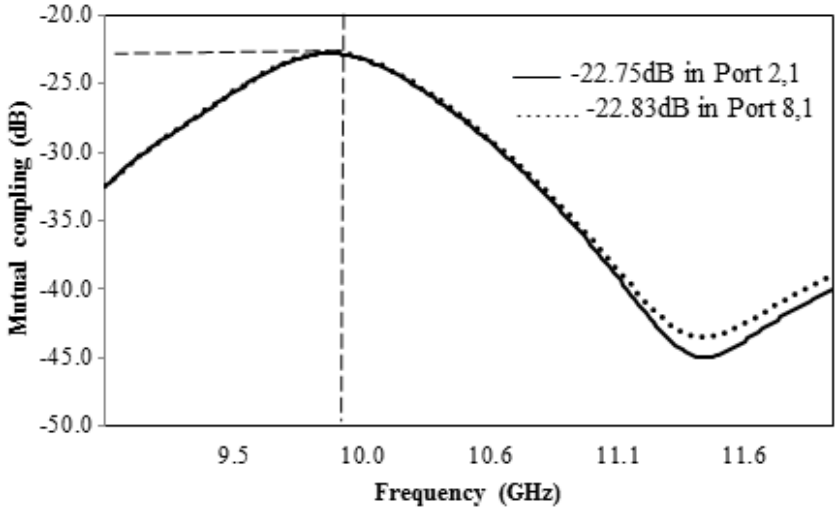


**Figure 11.** Mutual coupling between 8 element MCAA.

**Table 1.** Comparison of antenna parameters for various sizes of circular arrays.

| | 4 Elements | 8 Elements | 16 Elements |
|---|---|---|---|
| $\beta(deg)$ | 90 | 45 | 22.5 |
| Interelement spacing $d$ | $1.35\lambda$ | $0.67\lambda$ | $0.33\lambda$ |
| Radius of MCAA (cm) | 2.6 | 2.6 | 5 |
| Side lobe level (dB) | –1.5 | –5.75 | –4.84 |
| FNBW (deg) | 30 | 48 | 24 |
| HPBW (deg) | 28 | 24 | 26 |
| Return loss (dB) | 15.8 to 16.3 | 15.3 to 15.5 | 15.6 to 15. 8 |
| Maximum gain (dB) | 10.41 | 12.8 | 14.77 |

### 4.2. DC coefficients

We have adopted the Davies transformation method to demonstrate the DC excitations in MCCAs [26]. According to the phase mode theory, the CAA excitation coefficients $J_n$ are treated in the same linear array (LA). Thus, DC coefficients are used to find the magnitude of an element with respect to the phase as LA. The analysis technique was classified with the desired SLL. Here, the SLL is chosen as 20 dB for 8 element MCAA with spacing of $d = 0.67\lambda$. The even mode of an array factor is given by

$$AF = 2\sum_{n=1}^{N} V_n cos?(2n-1)kdcos? \tag{7}$$

The Chebyshev polynomials are given by

$$F_n(x) = \cosh[N\cos^{-1}(x)], \text{ For } -1 \le x \le +1 \text{ of } N \text{ even mode } 5 \tag{8}$$

and

$$x_o = cosh\left[\frac{cosh^{-1}V_o}{N-1}\right],$$

where $x_o$ corresponds to the direction of the major lobe, $N$ number of elements, and $(N-1)$ the order of the array factor. Table 2 shows the calculated array factor for $V_n$ along with phase angles for the circular array.

Figures 12a and 12b show the calculated array factor for DC coefficients for the 8 elements and computed coefficients for the elements in the $x$-axis at equal spacing, respectively. These magnitudes of $V_n$ are applied to get an 8 element MCAA with stable side lobes level of 20 dB.

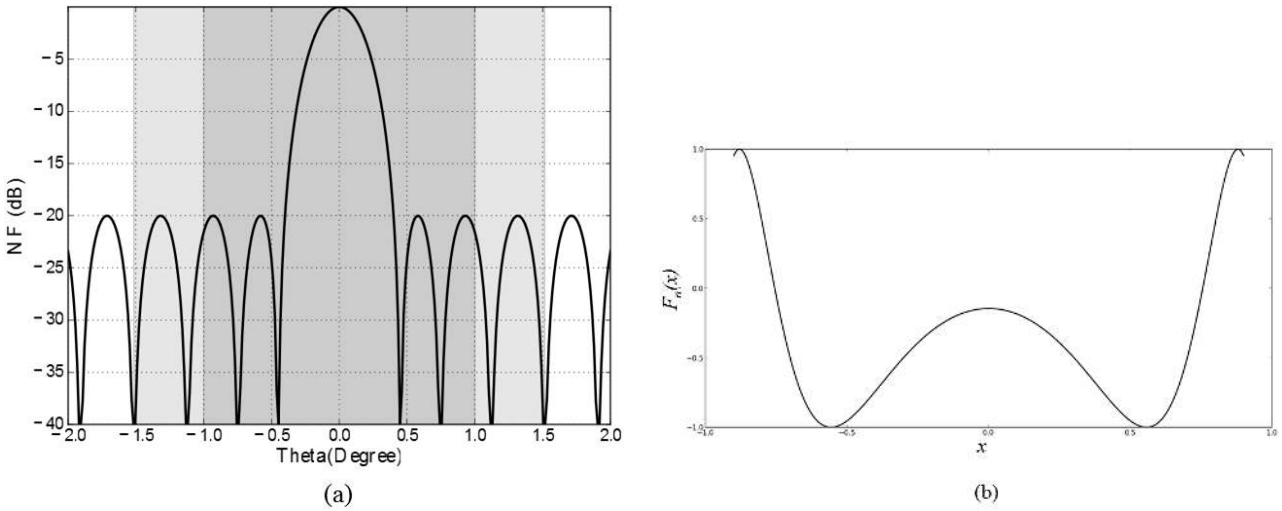


**Figure 12.** Dolph–Chebyshev polynomials for (a) 8th order AF, (b) magnitude of corresponding Chebyshev polynomial $F_n(x)$.

**Table 2.** Dolph–Chebyshev coefficients for 8 element array with element spacing $d = 0.67\ \lambda$.

| Position of the element ($n$) | Magnitude ($V_n$) | Phase angle $\alpha_n$ (deg) |
|---|---|---|
| 1 | $V_1 = 0.308$ | $\alpha_1 = 0$ |
| 2 | $V_2 = 1.9719$ | $\alpha_2 = 45$ |
| 3 | $V_3 = 3.080$ | $\alpha_3 = 90$ |
| 4 | $V_4 = 3.787$ | $\alpha_4 = 135$ |

EM simulation of MCAA is performed with similar configurations as that uniform excitation case. Simulated radiation patterns at various azimuthal planes are illustrated in Figure 13. As expected, the side lobe level of 20 dB is achieved in MCAA in the first side lobe where uniform offers 4 dB. However, other side lobes are showing a gradual reduction up to 45 dB. This is due to the nature of the circular array and the nonisotropic nature of microstrip patches. The grating lobes, which are visible in $\phi = 45^\circ$, are well suppressed in comparison with uniform excitation. It is also observed in Figure 13 that a large asymmetry in azimuthal is visible for DC excitation while uniform excitation shows a high degree of circular symmetry along the azimuthal plane (in Figure 9). This is due to nonuniform excitation of elements in the circular axis. This similar technique can be extended to design various nonuniform arrays, such as Zolotarev, Bayliss, Taylor, etc. with radial symmetry and suppressed grating lobes; the circular arrays are suitable for direction finding application, such as radar.

Table 3 compares the performance of DC circular arrays with isotropic, nonisotropic (microstrip) uniform circular array, and Zolotarev circular array [36]. It is found that DC and Zolotarev arrays show high performance in many aspects. This is due to the nonuniform excitation along with the influence of Taylor-like distribution of UCA. It is worth noting that for the 8 element DC circular array, the HPBW increases hugely while changing the element spacing from $0.67\lambda$ to $0.5\lambda$. This could be due to the coupling effect and diameter of the circular array. It is reflected in the maximum gain of the DC array with a high value of 23.67 dB. Further enhancement

of SLL and maximum gain can be possible with an increase in the number of elements with optimum weight selection.

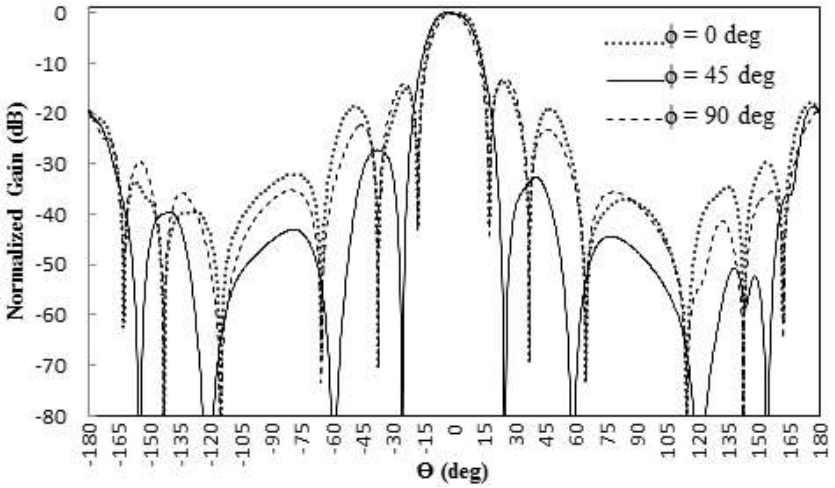


**Figure 13.** Gain pattern for 8 element MCAA with DC excitation.

**Table 3.** Performance comparison of circular arrays with uniform and nonuniform excitation.

| 5.1. Antenna parameters | 5.2. Uniform circular array with isotropic elements | 5.3. Uniform circular array with microstrip elements | 5.4. DC circular array with microstrip elements | 5.5. Zolotarev circular array with microstrip elements [36] | 5.6. DC circular array with nonisotropic elements [24] |
|---|---|---|---|---|---|
| Number of elements | 8 | 8 | 8 | 8 | 8 |
| Frequency (GHz) | 10 | 10 | 10 | 10 | 35 |
| Interelement spacing ($d$) | 0.67λ | 0.67λ | 0.67λ | 0.67λ | 0.5λ |
| Achieved side lobe level (dB) | NA | NA | 24.1 | 23.8 | 29.44 |
| Angular width (deg) | 22.5 | 12 | 6.3 | 6.3 | 18 |
| FNBW (deg) | 90 | 48 | 36 | 41 | 50 |
| Maximum gain (dB) | 12.0 | 12.8 | 23.67 | 20.66 | 15.9 |

## 5. Conclusion

In this paper, microstrip circular antenna arrays are demonstrated with DC excitations. The DC excitations are calculated for the SLL of 20 dB, with element spacing d $< 1\lambda$ to avoid grating lobes. First the uniform circular ring has been analyzed with isotropic, and later directional microstrip radiators are also introduced. It is observed that DC excitation shows a large improvement over uniform excitations. This is due to the careful integration of phase/look angles in the circular array with DC excitations. It is observed that grading lobes are emerging for the $d > 1\lambda$ case. The CAAs show excellent circular symmetry due to circular patch elements. This unique property is highly recommended for radar application.

## Acknowledgments

The authors would like to acknowledge the support given by Mohammed Zackriya. Also they acknowledge the Editor and anonymous reviewers, who helped to improve the manuscript in various aspects.

## References

[1] Fenn AJ, Temme DH, Delaney WP, Courtney WE. The development of phased-array radar technology. Lincoln Lab J 2000; 12: 321-340.

[2] Ares F, Franceschetti G, Mosig J, Vaccaro S, Vassal'lo J, Moreno E. Satellite communication with moving vehicles on earth: two prototype circular array antennas. Microw Opt Techn Let 2003; 391: 14-16.

[3] Rahim T, Davies D. Effect of directional elements on the directional response of circular antenna arrays. IEE Proc H 1982; 129: 18-22.

[4] Hidayat R, Rifai I, Widada W, Adi A. Doppler circular array antenna principle for determining azimuth angle of radio transmitter. In: IEEE 2011 Intelligent Signal Processing and Communications Systems (ISPACS) International Symposium; 07-09 Dec 2011; Bangkok, Thailand: IEEE. pp. 1-4.

[5] Sanudin R, Arslan T. Semi-circular antenna array for azimuth doa estimation. In: IEEE 2012 Antennas and Propagation Conference; 12–13 Nov 2012; Loughborough, United Kingdom: IEEE. pp. 1-4.

[6] Chu TS. On the use of uniform circular arrays to obtain omnidirectional patterns. IRE Transactions on Antennas and Propagation 1959; 7: 436-438.

[7] Josefsson L, Persson P. Conformal Array Antenna Theory and Design. 1st ed. Hoboken, NJ, USA: Wiley, 2006.

[8] Gerini G, Zappelli L. Multilayer array antennas with integrated frequency selective surfaces conformal to a circular cylindrical surface. IEEE T Antenn Propag 2015; 53: 2020-2030.

[9] Ram G, Mandal D, Kar P, Ghoshal SP. Design of non-uniform circular antenna arrays using firefly algorithm for side lobe level reduction. International Journal of Electrical, Computer, Electronics and Communication Engineering 2014; 8: 36-41.

[10] Askari M, Karimi M. Sector beam forming with uniform circular array antennas using phase mode transformation In: IEEE 2013 Electrical Engineering; 14–16 May 2013; Mashad, Iran: IEEE. pp. 1-6.

[11] Chatterjee A, Mahanti G. Side lobe reduction of a uniformly excited concentric ring array antenna using evolutionary algorithms. ICTACT J Communication Techn 2010; 1: 230-234.

[12] Balanis CA. Antenna Theory: Analysis and Design. 3rd ed. Hoboken, NJ, USA: John Wiley & Sons, 2012.

[13] Goossens R, Bogaert I, Rogier H. Phase-mode processing for spherical antenna arrays with a finite number of antenna elements and including mutual coupling. IEEE T Antenn Propag 2009; 57: 3783-3790.

[14] Yusuf Y, Gong X. A low-cost patch antenna phased array with analog beam steering using mutual coupling and reactive loading. IEEE Antenn Wirel Pr 2008; 7: 81-84.

[15] Breakall JK. Introduction to the three-dimensional frequency independent phased-array (3d-fipa)-a new class of phased array design. In: IEEE 1992 Antennas and Propagation Society International Symposium; 18–25 June 1992; California, USA: IEEE. pp. 1414-1417.

[16] Zinka SR. Arraytool: An open source python based package for array antenna analysis and design, 2010.

[17] Zinka SR, Jeong IB, Chun JH, Kim KP. A novel geometrical technique for determining optimal array antenna lattice configuration. IEEE T Antenn Propag 2010; 58: 404-412.

[18] Dolph CL. A current distribution for broadside arrays which optimizes the relationship between beam width and side-lobe level. Proc IRE 1946; 34: 335-348.

[19] Lau B, Leung Y. Analysis of Dolph-Chebyshev patterns for uniform linear arrays. SPL-TR-013, ATRI, Curtin Uni of Tech 1999; 181-185.

[20] Tseng CY, Griffiths LJ. A simple algorithm to achieve desired patterns for arbitrary arrays. IEEE T Signal Proc 1992; 40: 2737-2746.

[21] Stegen R. Excitation coefficients and beamwidths of tschebyscheff arrays. Proc IRE 1953; 41: 1671-1674.

[22] Safaai-Jazi A. A new formulation for the design of Chebyshev arrays. IEEE T Antenn Propag 1994; 42: 439-443.

[23] Thadeu G, Kohno R. A modified Dolph-Chebyshev approach for the synthesis of low side lobe beam patterns with adjustable beamwidth. IEEE T Antenn Propag 2003; 51: 3014-3017.

[24] Liu M, Feng ZR, Wu Q. Design of a millimeter-wave conformal low sidelobe microstrip antenna array on a cone surface. In: IEEE 2008 China-Japan Joint Microwave Conference; 10–12 Sep 2008; Shanghai, China: IEEE. pp. 121-124.

[25] Zhang Z, Fu M, Chang C. A 24 GHz microstrip array antenna. In: IEEE 2011 Proceedings of Computer Science and Network Technology Conference; 24–26 Dec 2011; Harbin, China: IEEE. pp. 214-217.

[26] Davies DA. Transformation between the phasing techniques required for linear and circular aerial arrays. Proc Inst Elec Eng 1965; 112: 2041-2045.

[27] Lau B, Leung Y. A Dolph-Chebyshev approach to the synthesis of array patterns for uniform circular arrays. In: IEEE 2000 Circuits and Systems (ISCAS) International Symposium; 28–31 May 2000; Geneva, Switzerland: IEEE. pp. 124-127.

[28] Naveen KS, Ayub KM, Nitendar K, Pourush PKS. LiTiMg ferrite substrate for circular array of circular patches under external magnetic field. Indian Journal of Science and Technology 2010; 3: 299-302.

[29] Railton C, Paul D, Craddock I. Analysis of a 17 element conformal array of stacked circular patch elements using an enhanced FDTD approach. IEE P-Microw Anten P 2003; 150: 153-158. Kong J. Analysis of a circular microstrip disk antenna with a thick dielectric substrate. IEEE T Antenn Propag 1981; 29: 68-76.

[30] Dahele J, Lee K. Effect of substrate thickness on the performance of a circular-disk microstrip antenna. IEEE T Antenn Propag 1983; 31: 358-360.

[31] Bhattacharyya A. Effects of finite ground plane on the radiation characteristics of a circular patch antenna. IEEE T Antenn Propag 1990; 38: 152-159.

[32] Shen L, Long S, Allerding M, Walton M. Resonant frequency of a circular disc, printed-circuit antenna. IEEE T Antenn Propag 1977; 25: 595-596.

[33] Mei K. Unimoment method of solving antenna and scattering problems. IEEE T Antenn Propag 1974; 22: 760-766.

[34] Derneryd AG. Analysis of the microstrip disk antenna element. IEEE T Antenn Propag 1979; 27: 660-664.

[35] Mohan KN, Kannadassan D, Zinka SR. Design and implementation of Dolph Chebyshev and Zolotarev circular antenna array. Indian Journal of Science and Technology 2016; 9: 1-9.